

Full counting statistics in disordered graphene at Dirac point: From ballistics to diffusion

A. Schuessler,¹ P. M. Ostrovsky,^{1,2} I. V. Gornyi,^{1,3,4} and A. D. Mirlin^{1,4,5,6}

¹ *Institut für Nanotechnologie, Karlsruher Institut für Technologie, 76131 Karlsruhe, Germany.*

² *L. D. Landau Institute for Theoretical Physics RAS, 119334 Moscow, Russia.*

³ *A. F. Ioffe Physico-Technical Institute, 194021 St. Petersburg, Russia.*

⁴ *DFG Center for Functional Nanostructures, Karlsruher Institut für Technologie, 76131 Karlsruhe, Germany.*

⁵ *Inst. für Theorie der Kondensierten Materie, Karlsruher Institut für Technologie, 76131 Karlsruhe, Germany.*

⁶ *Petersburg Nuclear Physics Institute, 188300 St. Petersburg, Russia.*

The full counting statistics of the charge transport through an undoped graphene sheet in the presence of smooth disorder is studied. At the Dirac point both in clean and diffusive limits, transport properties of a graphene sample are described by the universal Dorokhov distribution of transmission probabilities. In the crossover regime, deviations from universality occur which can be studied analytically both on ballistic and diffusive sides. In the ballistic regime, we use a diagrammatic technique with matrix Green functions. For a diffusive system, the sigma model is applied. Our results are in good agreement with recent numerical simulations of electron transport in disordered graphene.

PACS numbers: 73.63.-b, 73.22.-f

I. INTRODUCTION

Electron transport in graphene remains a field of intense experimental and theoretical activity^{1,2}. The hallmark of graphene is the massless Dirac character of low-energy electron excitations. This gives rise to remarkable physical properties of this system distinguishing it from conventional two-dimensional metals. The most remarkable effects arise when the chemical potential is located in a close vicinity of the neutrality (Dirac) point. In particular, a short-and-wide sample (with width W much exceeding the length L) of clean graphene exhibits at the Dirac point pseudo-diffusive charge transport,³ with “conductivity” $4e^2/\pi h$ and with counting statistics (characterizing fluctuations of current) equivalent to that of a diffusive wire.^{4–7} In particular, the Fano factor (the shot noise power divided by the current) takes the universal value $F = 1/3$ that coincides with the well-known result for a diffusive metallic wire.⁸ This is at odds with usual clean metallic systems, where the conductance (rather than conductivity) is independent of L and the shot noise is absent ($F = 0$). The reason behind these remarkable peculiarities of transport in clean graphene at the Dirac point is linearly vanishing density of states. This implies that the current is mediated by evanescent rather than propagating modes. The above theoretical predictions have been confirmed in measurements of conductance and noise in ballistic graphene flakes.^{9–11} Recent advances in preparation and transport studies of suspended graphene samples also indicate that the system may be in the ballistic regime.^{12,13}

Effects of impurities on transport properties of graphene are highly unusual as well. In contrast to conventional metals, ballistic graphene near the Dirac point conducts better when potential impurities are added.^{14–16} Quantum interference in disordered graphene is also highly peculiar due to the Dirac nature of the carri-

ers. In particular, in the absence of intervalley scattering, the minimal conductivity¹⁷ $\sim e^2/h$ is “topologically protected” from quantum localization.¹⁸ The exact value of the conductivity of such a system at the Dirac point depends on the type of intravalley scattering (random scalar or vector potential, or random mass, or their combination). For the case of random potential only (which is experimentally realized by charged scatterers) the conductivity in fact increases logarithmically with the length L , in view of antilocalization.^{14,19–22}

In our previous work¹⁶, we have studied the evolution of conductance of a short-and-wide graphene sample from the ballistic to the diffusive regime. We have also shown that the leading disorder-induced correction to the noise and full counting statistics in the ballistic regime is completely governed by the renormalization of the conductance. This implies, in particular, that the Fano factor $1/3$ remains unaffected to this order. Indeed, the experiments^{10,23} give Fano factor values in the vicinity of $1/3$ at the Dirac point for different system lengths L . One could thus ask whether deviations from this value should be expected at all.

In this work we present a detailed analysis of the shot noise and the full counting statistics in samples with long-range (no valley mixing) disorder. We show that to second order in the disorder strength a correction to the universal counting statistics of the ballistic graphene does arise. We calculate this correction and demonstrate that it suppresses the Fano factor below the value $1/3$. For the case of random scalar potential, we also analyze the opposite limit of large L when the system is deep in the diffusive regime. Generalizing the analysis of weak-localization effects on the counting statistics by Nazarov²⁴, we find that the Fano factor returns to the value of $1/3$ from below with increasing L . The approach to $1/3$ is however logarithmically slow, These results compare well with recent numerical works^{20,21} and particu-

larly with the most detailed study by Tworzydło *et al.*²²

The structure of the paper is as follows. In the Sec. II, we describe the general matrix Green function formalism and its application to the problem of full counting statistics. The model for graphene setup and disorder is introduced in Sec. III. We proceed with applying matrix Green function method to the calculation of the distribution of transmission probabilities of the clean graphene sample in Sec. IV. In Sec. V we evaluate perturbative disorder corrections to the full counting statistics in ballistic regime. Diffusive transport through disordered graphene is considered in Sec. VI within the sigma-model approach. The paper is concluded by Sec. VII summarizing the main results. Technical details of the calculation are presented in three appendices.

II. MATRIX GREEN FUNCTION FORMALISM

We begin with the general presentation of the matrix Green function approach to the full counting statistics of a quasi-one-dimensional system. This formalism was developed by Nazarov in Ref. 25.

Consider a quasi-one-dimensional sample attached to two perfect metallic leads. Transport characteristics of the system are encoded in the matrix of transmission amplitudes t_{mn} , where the indices enumerate conducting channels (quantized transverse modes) in the leads. Eigenvalues of the matrix $\hat{t}^\dagger \hat{t}$ determine transmission probabilities of the system (we use the “hat” notation for matrices in the space of channels). Our main goal is to calculate the distribution of these transmission probabilities. The full counting statistics of the charge transport is given by the moments of this distribution or, equivalently, by the distribution itself. The first two moments of the transferred charge provide the conductance (by Landauer formula) and the Fano factor

$$G = \frac{e^2}{h} \text{Tr} \hat{t}^\dagger \hat{t}, \quad F = 1 - \frac{\text{Tr}(\hat{t}^\dagger \hat{t})^2}{\text{Tr} \hat{t}^\dagger \hat{t}}. \quad (1)$$

The starting point of our consideration is the relation between the matrix of transmission probabilities and the Green function of the system,

$$t_{mn} = i\sqrt{v_m v_n} G_{mn}^A(x, x'), \quad (2)$$

Here $v_{m,n}$ are velocities in the m th and n th channel. The Green function is taken in the mixed representation with real-space coordinates in the longitudinal direction and channel indices in transverse direction. The positions x and x' should be taken in the left and right lead respectively in order to obtain the transmission matrix of the full system. The conjugate matrix \hat{t}^\dagger is related to the retarded Green function by a similar identity.

The Green functions are defined in the standard way as

$$(\epsilon - \hat{H} \pm i0)\hat{G}^{R,A}(x, x') = \delta(x - x')\hat{1}, \quad (3)$$

with energy ϵ and Hamiltonian \hat{H} , the latter being an operator acting both on x and in the channel space.

With the help of Eq. (2) we can express all the moments of transmission distribution in terms of the Green functions,

$$\text{Tr} (\hat{t}^\dagger \hat{t})^n = \text{Tr} [\hat{v} \hat{G}^A(x, x') \hat{v} \hat{G}^R(x', x)]^n. \quad (4)$$

where \hat{v} is the velocity operator and x and x' lie in the left and right lead respectively. For the first moment, $n = 1$, the above identity establishes an equivalence of the Landauer and Kubo representations for conductance.

The complete statistics of the transmission eigenvalues can be represented by the generating function

$$\mathcal{F}(z) = \sum_{n=1}^{\infty} z^{n-1} \text{Tr} (\hat{t}^\dagger \hat{t})^n = \text{Tr} [\hat{t}^{-1} \hat{t}^{\dagger-1} - z]^{-1}. \quad (5)$$

Once this function is known, all the moments of transmission distribution are easy to obtain by expanding the generating function in series at $z = 0$. An efficient method yielding the whole generating function was proposed in Ref. 25. It amounts to calculating the matrix Green function defined by the following equation:

$$\begin{pmatrix} \epsilon - \hat{H} + i0 & -\sqrt{z}\hat{v}\delta(x - x_L) \\ -\sqrt{z}\hat{v}\delta(x - x_R) & \epsilon - \hat{H} - i0 \end{pmatrix} \check{G}(x, x') = \delta(x - x')\hat{1}. \quad (6)$$

The parameter z here corresponds to the source field mixing retarded and advanced components of the matrix Green function. The positions x_L and x_R , where the source field is applied, lie within the left and right lead respectively. We will refer to this specific matrix structure as the RA (retarded – advanced) space and denote such a matrices with the “check” notation.

The main advantage of the matrix Green function defined by Eq. (6) is the following concise expression for the generating function of transmission probabilities:

$$\begin{aligned} \mathcal{F}(z) &= \frac{1}{\sqrt{z}} \text{Tr} \left[\begin{pmatrix} 0 & 0 \\ \hat{v} & 0 \end{pmatrix} \check{G}(x_R, x_R) \right] \\ &= \frac{1}{\sqrt{z}} \text{Tr} \left[\begin{pmatrix} 0 & \hat{v} \\ 0 & 0 \end{pmatrix} \check{G}(x_L, x_L) \right]. \end{aligned} \quad (7)$$

The validity of this equation can be directly checked by expanding the Green function in powers of z with the help of perturbation theory and comparing this expansion termwise with Eq. (5). The equivalence of these two expansions is provided by the identity (4).

Another and, probably, most intuitive representation of the full counting statistics is given by the distribution function of transmission probabilities $P(T)$. This function takes its simplest form when expressed in terms of the parameter λ related to the transmission probability by $T = 1/\cosh^2 \lambda$. In terms of λ the probability density is defined by the identity $P(T)dT = P(\lambda)d\lambda$. The definition of the generating function, Eq. (5), implies a

trace involving all transmission probabilities. With the distribution function of these probabilities we can express $\mathcal{F}(z)$ by the integral

$$\mathcal{F}(z) = \int_0^\infty \frac{P(\lambda)d\lambda}{\cosh^2 \lambda - z}. \quad (8)$$

The function $\mathcal{F}(z)$ has a branch cut discontinuity in the complex z plane running from 1 to $+\infty$. The jump of the function across the branch cut determines the distribution function [see Ref. 16 for derivation]:

$$P(\lambda) = \frac{\sinh 2\lambda}{2\pi i} [\mathcal{F}(\cosh \lambda + i0) - \mathcal{F}(\cosh \lambda - i0)]. \quad (9)$$

In other words, Eq. (8) solves the Riemann-Hilbert problem defined by Eq. (9).

The generating function $\mathcal{F}(z)$ can be related to the “free energy” of the system in the “external” source field. The free energy is defined in terms of the functional determinant

$$\Omega = \text{Tr} \ln \check{G}, \quad \mathcal{F} = \frac{\partial \Omega}{\partial z}. \quad (10)$$

The free energy can be calculated by standard diagrammatic methods and hence provides a very convenient representation of the full counting statistics. It is also convenient to parametrize the argument of the free energy by the angle ϕ according to $z = \sin^2(\phi/2)$.

Thus we have three equivalent representations of the full counting statistics by the functions $\mathcal{F}(z)$, $P(\lambda)$, and $\Omega(\phi)$. In this paper we calculate the transport characteristics of a disordered graphene sample in terms of its free energy $\Omega(\phi)$. The two other functions can be found with the help of identities

$$\mathcal{F}(z) = \frac{2}{\sin \phi} \left. \frac{\partial \Omega}{\partial \phi} \right|_{\phi=2 \arcsin \sqrt{z}}, \quad (11)$$

$$P(\lambda) = \frac{2}{\pi} \text{Re} \left. \frac{\partial \Omega}{\partial \phi} \right|_{\phi=\pi+2i\lambda}. \quad (12)$$

The first of these relations directly follows from Eq. (10) while the second one is the result of the substitution of Eq. (11) into Eq. (9).

The two most experimentally relevant quantities contained in the full counting statistics, namely, conductance and Fano factor, Eq. (1), can be expressed in terms of any of the functions introduced above. Then the following expressions for the conductance and the Fano factor hold:

$$G = \frac{2e^2}{h} \left. \frac{\partial^2 \Omega}{\partial \phi^2} \right|_{\phi=0}, \quad (13)$$

$$F = \frac{1}{3} - \frac{2}{3} \left. \frac{\partial^4 \Omega / \partial \phi^4}{\partial^2 \Omega / \partial \phi^2} \right|_{\phi=0}. \quad (14)$$

We will apply the matrix Green function formalism outlined in this section to the problem of full counting

statistics of a disordered graphene sample. Our strategy is as follows. First, we calculate the matrix Green function of a clean rectangular graphene sample and obtain the full counting statistics with the help of Eq. (7). Then we introduce disorder in the model perturbatively. Evaluation of the free energy by diagrammatic methods yields disorder corrections to the full counting statistics of a clean sample.

III. MODEL

We will adopt the single-valley model of graphene. More specifically, we will consider scattering of electrons only within a single valley and neglect intervalley scattering events. Indeed, a number of experimental results show that in many graphene samples the dominant disorder scatters electrons within the same valley. First, this disorder model is supported by the odd-integer quantization^{1,17,26} of the Hall conductivity, $\sigma_{xy} = (2n+1)2e^2/h$, representing a direct evidence²⁷ in favor of smooth disorder which does not mix the valleys. The analysis of weak localization also corroborates the dominance of intra-valley scattering²⁸. Furthermore, the observation of the linear density dependence¹ of graphene conductivity away from the Dirac point can be explained if one assumes that the relevant disorder is due to charged impurities and/or ripples.^{19,29–32} Due to the long-range character of these types of disorder, the intervalley scattering amplitudes are strongly suppressed and will be neglected in our treatment. Finally, apparent absence of localization at the Dirac point down to very low temperatures^{17,26,33} points to some special symmetry of disorder. One realistic candidate model is the long-range randomness which does not scatter between valleys^{18,34}.

The single-valley massless Dirac Hamiltonian of electrons in graphene has the form (see, e.g., Ref. 2)

$$H = v_0 \boldsymbol{\sigma} \mathbf{p} + V(x, y), \quad V(x, y) = \sigma_\mu V_\mu(x, y). \quad (15)$$

Here σ_μ (with $\mu = 0, x, y, z$) are Pauli matrices acting on the electron pseudospin degree of freedom corresponding to the sublattice structure of the honeycomb lattice, $\boldsymbol{\sigma} \equiv \{\sigma_x, \sigma_y\}$, and the Fermi velocity is $v_0 \approx 10^8$ cm/s. The random part $V(x, y)$ is in general a 2×2 matrix in the sublattice space. Below we set $\hbar = 1$ and $v_0 = 1$ for convenience.

We will calculate transport properties of a rectangular graphene sample with the dimensions $L \times W$. The contacts are attached to the two sides of the width W separated by the distance L . We fix the x axis in the direction of current, Fig. 1, with the contacts placed at $x = 0$ and $x = L$. We assume $W \gg L$, which allows us to neglect the boundary effects related to the edges of the sample that are parallel to the x axis (at $y = \pm W/2$).

Following Ref. 5, metallic contacts are modelled as highly doped graphene regions described by the same Hamiltonian (15). In other words, we assume that the

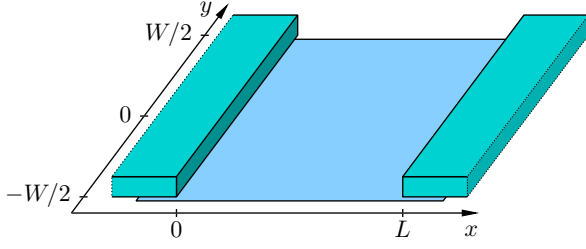


FIG. 1: (Color online) Schematic setup for two-terminal transport measurements. Graphene sample of dimensions $L \times W$ is placed between two parallel contacts. We assume $W \gg L$ throughout the paper.

chemical potential E_F in the contacts is shifted far from the Dirac point. In particular, $E_F \gg \epsilon$, where ϵ is the chemical potential inside the graphene sample counted from the Dirac point. (All our results are independent of the sign of energy, thus we assume $\epsilon > 0$ throughout the paper.) We also assume zero temperature, that is justified provided $TL \ll 1$.

With the boundary conditions specified above, we are able to calculate explicitly the matrix Green function (6) for a clean graphene sample [$V(x, y) = 0$] at zero energy. This calculation is outlined in Appendix A [see Eq. (A7)]. Using this Green function, we will study disorder effects in the framework of the diagrammatic technique for the free energy.

IV. ELECTRON TRANSPORT IN CLEAN GRAPHENE

In this section we apply the matrix Green function formalism developed in Sec. II to the case of clean graphene. These results will play the role of the zeroth approximation for our perturbation theory.

The matrix Green function is derived in Appendix A. The generating function for the full counting statistics is given by Eq. (7). With the Green function (A7), we obtain

$$\mathcal{F}_0(\sin^2 \frac{\phi}{2}) = \frac{W}{\sin \frac{\phi}{2}} \text{Tr} \left[\begin{pmatrix} 0 & \sigma_x \\ 0 & 0 \end{pmatrix} \check{G}(0, 0; 0) \right] = \frac{W}{\pi L} \frac{\phi}{\sin \phi}. \quad (16)$$

The corresponding dependence of the free energy on the source field ϕ follows from integration of Eq. (11). This yields a simple quadratic function

$$\Omega_0(\phi) = \frac{W\phi^2}{4\pi L}. \quad (17)$$

This remarkably simple result reveals the convenience of the source field parametrization $z = \sin^2(\phi/2)$. The clean sample responds linearly to the “external” field ϕ . The distribution of transmission probabilities given by Eq. (12) is just a constant, $P_0(\lambda) = W/\pi L$, in terms of λ . This means the distribution acquires the Dorokhov form⁴

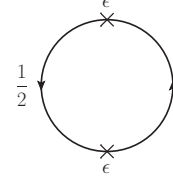


FIG. 2: Lowest energy correction to the free energy of the system.

characteristic for disordered metallic wires

$$P_0(T) = \frac{W}{2\pi L} \frac{1}{T\sqrt{1-T}}. \quad (18)$$

Hence electron transport in clean graphene at the Dirac point is often called pseudodiffusive.

Let us now calculate an energy correction to the pseudodiffusive transport regime. In the vicinity of the Dirac point (we assume $\epsilon L \ll 1$), we can account for finite energy ϵ by means of perturbation theory. The linear term is absent due to particle-hole symmetry of the Dirac point. The lowest non-vanishing correction appears in the ϵ^2 order and is given by the single diagram Fig. 2,

$$\Omega_\epsilon = \frac{W\epsilon^2}{2} \int_0^L dx dx' \int_{-\infty}^{\infty} dy \text{Tr} G(x, x'; y) G(x', x; -y). \quad (19)$$

This integral of the product of two Green functions is calculated in Appendix B. The result takes the form

$$\Omega_\epsilon = \frac{W(\epsilon L)^2}{\pi L \sin \frac{\phi}{2}} \frac{\partial}{\partial \phi} \left\{ \cos \frac{\phi}{2} \left[\psi \left(\frac{\pi + \phi}{2\pi} \right) + \psi \left(\frac{\pi - \phi}{2\pi} \right) \right] \right\}, \quad (20)$$

where ψ is the digamma function.

As explained above, the free energy Ω_ϵ contains information about the full counting statistics, i.e. all moments of the transferred charge. In particular, from Eqs. (13) and (14) we obtain the following results for the conductance and Fano factor:

$$G = \frac{4e^2}{\pi h} \frac{W}{L} [1 + c_1(\epsilon L)^2], \quad F = \frac{1}{3} [1 + c_2(\epsilon L)^2], \quad (21)$$

$$c_1 = \frac{35\zeta(3)}{3\pi^2} - \frac{124\zeta(5)}{\pi^4} \approx 0.101, \quad (22)$$

$$c_2 = -\frac{28\zeta(3)}{15\pi^2} - \frac{434\zeta(5)}{\pi^4} + \frac{4572\zeta(7)}{\pi^6} \approx -0.052. \quad (23)$$

These expressions coincide with the results of Ref. 16 obtained within an alternative (transfer-matrix) approach.

V. DISORDERED GRAPHENE: BALLISTIC LIMIT

Let us now include the random part $V(x, y)$ of the Hamiltonian (15) into consideration. There are in total

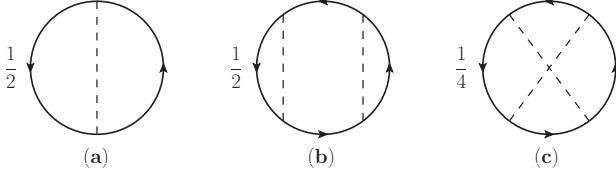


FIG. 3: Loop diagrams for the disorder corrections to the ground state energy Ω , (a) first-order, (b) and (c) second-order.

four different types of disorder within the single valley Dirac model: V_0 is the random potential (charged impurities in the substrate), V_x and V_y correspond to the random vector potential (e.g. long-range corrugations), and V_z is the random mass. We will assume the standard Gaussian type of disorder characterized by the correlation function

$$\langle V_\mu(\mathbf{r})V_\nu(\mathbf{r}') \rangle = 2\pi\delta_{\mu\nu}w_\mu(|\mathbf{r} - \mathbf{r}'|). \quad (24)$$

The functions $w_\mu(r)$ depend only on the relative distance r and are strongly peaked near $r = 0$. Thus we deal with isotropic and nearly white-noise disorder. However, in order to accurately treat ultraviolet divergencies arising in our calculation, we keep a small but finite disorder correlation length. The results will be expressed in terms of four integral constants characterizing the disorder strength

$$\alpha_\mu = \int d\mathbf{r} w_\mu(|\mathbf{r}|). \quad (25)$$

Within the specified Gaussian disorder model, perturbative corrections to the free energy are given by the loop diagrams. The first and second order corrections are shown in Fig. 3. Dashed lines in these diagrams denote disorder correlation functions (24).

A. First-order correction

The first-order correction to the free energy $\Omega(\phi)$ is given by the loop diagram containing two Green functions and one impurity line, Fig. 3a. The Green function at coincident points diverges. That is why we keep a finite correlation length calculating the first-order diagram. Assuming the separation between two vertices of the diagram is given by the vector δ , we obtain the expression

$$\Omega_a = \int d\delta \sum_\mu w_\mu(|\delta|)\Omega_a^{(\mu)}, \quad (26)$$

$$\delta\Omega_a^{(\mu)} = \pi \int d\mathbf{r} \text{Tr} \left[\sigma_\mu \tilde{G}(\mathbf{r}, \mathbf{r} + \delta) \sigma_\mu \tilde{G}(\mathbf{r} + \delta, \mathbf{r}) \right]. \quad (27)$$

Now we substitute the Green function from Eq. (A7) and expand the correction to the free energy in powers of δ .

For the four possible disorder types, this yields

$$\Omega_a^{(0),(z)} = \frac{\pi W}{2L^2} \int_0^L dx \left[\frac{-1}{2 \sin^2 \frac{\pi x}{L}} \pm \left(\frac{\delta_x^2 - \delta_y^2}{6\delta^2} + \frac{\delta_y^2 \phi^2}{\pi^2 \delta^2} \right) \right], \quad (28)$$

$$\Omega_a^{(x),(y)} = \frac{\pi W}{L^2} \int_0^L dx \left[\frac{-1}{4 \sin^2 \frac{\pi x}{L}} \pm \left(\frac{1}{12} + \frac{\delta_x^2 - \delta_y^2}{\pi^2 \delta^4} \right) \right]. \quad (29)$$

In these expressions we encounter two types of divergent terms: one with negative power of δ and one with an integral of $\sin^{-2}(\pi x/L)$, which diverges at $x = 0$ and $x = L$. These terms, however, are free of the source parameter ϕ and hence do not change any observables. The ϕ -dependent terms are finite and, after integrating over δ in Eq. (26), yield the simple result:³⁵

$$\Omega_a = \text{const} + (\alpha_0 - \alpha_z) \frac{W\phi^2}{4\pi L}. \quad (30)$$

It provides a linear (in α_μ) correction to the free energy of the clean sample, Eq. (17), merely changing the overall prefactor (conductance) but preserving the quadratic dependence on ϕ and hence the form of the Dorokhov distribution. Thus the linear disorder correction does not destroy the pseudodiffusive character of transport in graphene at the Dirac point.

B. Second-order corrections

Since the lowest disorder correction (30) preserves the form of the Dorokhov distribution, we proceed with higher order corrections. Our aim is to find a deviation from the pseudodiffusive transport. The second-order correction to the free energy is due to the diagrams Fig. 3b and 3c. The diagram with parallel impurity lines (Fig. 3b) yields

$$\Omega_b = \int d\delta d\delta' \sum_{\mu,\nu} w_\mu(|\delta|)w_\nu(|\delta'|)\Omega_b^{(\mu\nu)}, \quad (31)$$

$$\Omega_b^{(\mu\nu)} = 2\pi^2 \int d\mathbf{r} d\mathbf{r}' \text{Tr} \left[\sigma_\mu G(\mathbf{r}, \mathbf{r} + \delta) \sigma_\mu G(\mathbf{r} + \delta, \mathbf{r}') \right. \\ \left. \times \sigma_\nu G(\mathbf{r}', \mathbf{r}' + \delta') \sigma_\nu G(\mathbf{r}' + \delta', \mathbf{r}) \right]. \quad (32)$$

Using the Green function from Eq. (A7), we expand the correction to the free energy in powers of δ and δ' . Then we drop all ϕ -independent terms and average with respect to the directions of δ and δ' . The following four

contributions to the free energy are non zero:

$$\begin{aligned}\Omega_b^{(00)} &= \Omega_b^{(zz)} = -\Omega_b^{(0z)} = -\Omega_b^{(z0)} \\ &= \frac{W\phi^2}{64L^4} \int_0^L dx dx' \int_{-\infty}^{\infty} dy \\ &\times \left[\frac{1}{\sin^2 \frac{\pi(x+x'+iy)}{2L}} + \frac{1}{\sin^2 \frac{\pi(x-x'+iy)}{2L}} + \text{c.c.} \right].\end{aligned}\quad (33)$$

After integrating with respect to x and x' the above expression vanishes. Thus we conclude that the diagram Fig. 3b gives no contribution to the free energy,

$$\Omega_b = 0. \quad (34)$$

Let us now consider the diagram Fig. 3c with crossed impurity lines. This diagram contains no Green functions at coincident points and hence does not require regularization. We can replace disorder correlation functions w_μ by equivalent delta-functions and obtain

$$\Omega_c = \sum_{\mu\nu} \alpha_\mu \alpha_\nu \Omega_c^{(\mu\nu)}, \quad (35)$$

$$\Omega_c^{(\mu\nu)} = \pi^2 \int d\mathbf{r} d\mathbf{r}' \text{Tr} \left[\sigma_\mu \check{G}(\mathbf{r}, \mathbf{r}') \sigma_\nu \check{G}(\mathbf{r}', \mathbf{r}) \right]^2. \quad (36)$$

With the Green function (A7) we find the following contribution to the sum in Eq. (35):

$$\begin{aligned}\Omega_c^{(00)} &= \Omega_c^{(0z)} = \Omega_c^{(z0)} \\ &= \frac{\pi^2 W}{64L^4} \int_0^L dx dx' \int_{-\infty}^{\infty} dy \cosh \frac{2\phi y}{L}\end{aligned}\quad (37)$$

$$\begin{aligned}&\times \left(\frac{1}{\left| \sin \frac{\pi(x+x'+iy)}{2L} \right|^2} - \frac{1}{\left| \sin \frac{\pi(x-x'+iy)}{2L} \right|^2} \right)^2, \\ \Omega_c^{(zz)} &= \Omega_c^{(00)} + \frac{\pi^2 W}{8L^4} \int_0^L dx dx' \int_{-\infty}^{\infty} dy \cosh \frac{2\phi y}{L} \\ &\times \left| \sin \frac{\pi(x+x'+iy)}{2L} \sin \frac{\pi(x-x'+iy)}{2L} \right|^{-2}.\end{aligned}\quad (38)$$

Two-dimensional integrals with respect to x and x' are straightforward due to periodicity of the integrand. As a result, the free energy is expressed as a single y integral:

$$\begin{aligned}\Omega_c &= \frac{\pi^2 W}{8L^2} \int_{-\infty}^{\infty} dy \frac{\cosh(2\phi y/L)}{\sinh^2(\pi y/L)} \left[(\alpha_0 + \alpha_z)^2 \coth \left| \frac{\pi y}{L} \right| \right. \\ &\quad \left. - (\alpha_0 + 3\alpha_z)(\alpha_0 - \alpha_z) \right].\end{aligned}\quad (39)$$

This integral diverges at $y = 0$. Expanding near this point, we find that the integrand behaves as $(L/|y|)^3 + 2\phi^2 L/|y|$. The most singular part is ϕ -independent and hence unobservable. Integral of the second term diverges

logarithmically and multiplies ϕ^2 . This gives a logarithmic correction to the conductance of the system preserving the pseudodiffusive form of the transmission distribution. Let us cut off the logarithmic integral at some ultraviolet scale $y = a$ that is the smallest scale where the massless Dirac model with Gaussian white-noise disorder applies, e.g. the scale of the disorder correlation length or lattice spacing in graphene. The upper cut-off is already embedded in the integrand of Eq. (39): the small y expansion is valid for $y \lesssim L$. Thus we can isolate the divergent part of the integral (39) and the remaining Ω_c correction, which has a non-trivial dependence on ϕ .

$$\begin{aligned}\Omega_c &= \frac{W\phi^2}{4\pi L} \left\{ (\alpha_0 + \alpha_z)^2 [2 \ln(L/a) + \omega_1(\phi)] \right. \\ &\quad \left. + (\alpha_0 + 3\alpha_z)(\alpha_0 - \alpha_z) \omega_2(\phi) \right\}.\end{aligned}\quad (40)$$

Since the logarithmic term in the free energy contains an ultraviolet parameter a defined up to a model-dependent constant, the functions $\omega_{1,2}(\phi)$ are fixed up to an arbitrary constant. With this accuracy, we find

$$\begin{aligned}\omega_1(\phi) &= \frac{\pi^3}{2L\phi^2} \int_{-\infty}^{\infty} dy \frac{\cosh \frac{\pi y}{L}}{\sinh^3 \left| \frac{\pi y}{L} \right|} \left(\cosh \frac{2\phi y}{L} - 1 - \frac{2\phi^2 y^2}{L^2} \right) \\ &= \text{const} - \psi(\phi/\pi) - \psi(-\phi/\pi),\end{aligned}\quad (41)$$

$$\begin{aligned}\omega_2(\phi) &= -\frac{\pi^3}{2L\phi^2} \int_{-\infty}^{\infty} dy \frac{\cosh(2\phi y/L) - 1}{\sinh^2(\pi y/L)} \\ &= \text{const} + \pi^2 \frac{\phi \cot \phi - 1}{\phi^2}.\end{aligned}\quad (42)$$

The logarithmic correction in Eq. (40) can be included into an effective L -dependence of the disorder strength parameters α_μ by renormalization group (RG) methods. The model of two-dimensional massless Dirac fermions subject to Gaussian disorder and its logarithmic renormalization appeared in various contexts. In particular, disorder renormalization in graphene was considered in Refs. 16,32,36. One-loop RG equations for effective disorder couplings as functions of a running scale Λ are

$$\frac{\partial \alpha_0}{\partial \ln \Lambda} = 2(\alpha_0 + \alpha_z)(\alpha_0 + \alpha_x + \alpha_y), \quad (43a)$$

$$\frac{\partial \alpha_x}{\partial \ln \Lambda} = \frac{\partial \alpha_y}{\partial \ln \Lambda} = 2\alpha_0 \alpha_z, \quad (43b)$$

$$\frac{\partial \alpha_z}{\partial \ln \Lambda} = 2(\alpha_0 + \alpha_z)(-\alpha_z + \alpha_x + \alpha_y). \quad (43c)$$

Parameters defined in Eq. (25) serve as initial conditions for the RG equations at an ultraviolet scale a . Integrating Eqs. (43) up to the largest scale that is the system size L , we obtain effective disorder couplings $\tilde{\alpha}_\mu = \alpha_\mu(L)$ and automatically take into account all leading logarithmic contributions like the one in Eq. (40). This allows us to replace the disorder parameters in the free energy by their renormalized values and drop the logarithm from

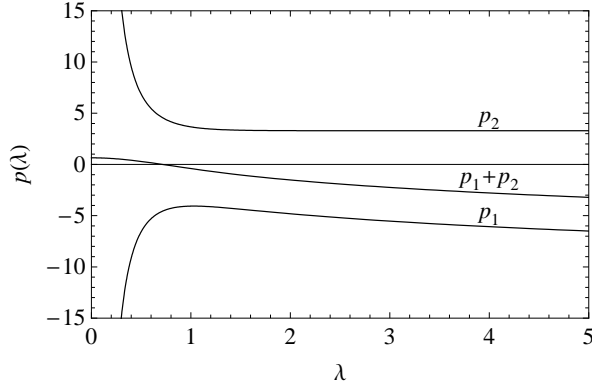


FIG. 4: Functions p_1 and p_2 entering the disorder correction to the distribution of transmission probabilities (45). In the case of random scalar potential (α_0), the distribution is determined by the sum $p_1 + p_2$ only.

Eq. (40). Collecting in this way the contributions (17), (30), and (40), we obtain the final expression for the free energy up to the second order in renormalized disorder parameters,

$$\Omega = \frac{W\phi^2}{4\pi L} \left[1 + \tilde{\alpha}_0 - \tilde{\alpha}_z + (\tilde{\alpha}_0 + \tilde{\alpha}_z)^2 \omega_1(\phi) + (\tilde{\alpha}_0 + 3\tilde{\alpha}_z)(\tilde{\alpha}_0 - \tilde{\alpha}_z) \omega_2(\phi) \right]. \quad (44)$$

Thus we have established a deviation from pseudodiffusive transport regime ($\Omega \sim \phi^2$) in the second order in disorder strength.

C. Corrections to the distribution function

Let us now derive a correction to the Dorokhov distribution function of transmission probabilities. In the λ representation, the distribution function is given by Eq. (12). Using the result (44), we obtain

$$P(\lambda) = \frac{W}{\pi L} \left[1 + \tilde{\alpha}_0 - \tilde{\alpha}_z + (\tilde{\alpha}_0 + \tilde{\alpha}_z)^2 p_1(\lambda) + (\tilde{\alpha}_0 + 3\tilde{\alpha}_z)(\tilde{\alpha}_0 - \tilde{\alpha}_z) p_2(\lambda) \right]. \quad (45)$$

Similarly to $\omega_{1,2}$, the functions $p_{1,2}(\lambda)$ are defined up to a model-dependent constant. From Eqs. (41) and (42) we obtain

$$p_1(\lambda) = \text{const} - 2 \text{Re} \frac{\partial}{\partial \lambda} \left[\lambda \psi \left(\frac{2i\lambda}{\pi} \right) \right], \quad (46a)$$

$$p_2(\lambda) = \text{const} + \frac{\pi^2}{2 \sinh^2(2\lambda)}. \quad (46b)$$

The functions p_1 and p_2 are shown in Fig. 4. (When the only disorder is α_0 , correction to the distribution function is given by the sum $p_1 + p_2$ also shown in the figure.)

The functions p_1 and p_2 cannot be used for direct calculation of transmission moments due to their divergence at $\lambda = 0$. This divergence signifies the break down of perturbative expansion in small values of disorder couplings close to $\lambda = 0$ (that is $T = 1$). Comparing disorder correction with the distribution in the clean sample, we conclude that the result (45) is valid provided $\lambda \gg \tilde{\alpha}$.

The deviation from pseudodiffusive transport regime can be experimentally demonstrated as a correction to the Fano factor $F = 1/3$ characteristic to the diffusive systems. Divergence of the functions $p_{1,2}$ at $\lambda = 1$ prevents us from calculating transmission moments from the distribution function (45). However, we can obtain transport characteristics from the free energy (44) instead. With the help of Eq. (14), we find the Fano factor up to quadratic terms in the renormalized disorder strength,

$$F = \frac{1}{3} - \frac{16\zeta(3)}{\pi^2} (\tilde{\alpha}_0 + \tilde{\alpha}_z)^2 + \frac{8\pi^2}{45} (\tilde{\alpha}_0 + 3\tilde{\alpha}_z)(\tilde{\alpha}_0 - \tilde{\alpha}_z) \approx \frac{1}{3} - 0.194 \tilde{\alpha}_0^2 - 0.388 \tilde{\alpha}_0 \tilde{\alpha}_z - 7.212 \tilde{\alpha}_z^2. \quad (47)$$

Remarkably, any weak disorder, irrespective of its matrix structure, suppresses the Fano factor. [Note that the energy correction (21) is also negative.] The correction to the Fano factor increases with increasing sample length L due to renormalization (43). At some length l , referred to as the mean free path, one of the renormalized disorder couplings reach a value of order unity and the perturbative RG treatment breaks down. This signifies the crossover from ballistic to diffusive transport regime. Disorder correction to the Fano factor becomes strong in this crossover region. To go beyond the mean free path scale we resort to other methods designed for diffusive systems.

VI. DISORDERED GRAPHENE: DIFFUSIVE LIMIT

When the system size exceeds the mean free path, the sample exhibits diffusive electron transport. On a semiclassical level, the system can be characterized by its conductivity per square in this limit. At the ballistics-diffusion crossover the conductivity of graphene is close to the quantum value e^2/h . This signifies strong interference corrections to transport characteristics making semiclassical picture inadequate. These quantum effects lead to one of the four possible scenarios depending on the symmetry of disorder:

- (i) If the only disorder is random potential (α_0), the system possesses time inversion symmetry $H = \sigma_2 H^T \sigma_2$ and falls into symplectic symmetry class AII^{37,38}. Quantum corrections to the conductivity are positive, leading to good metallic properties (large dimensionless conductivity) at large scales.
- (ii) In the case of random vector potential $\alpha_{x,y}$, the only symmetry of the problem is chirality, $H =$

$-\sigma_3 H \sigma_3$, signifying the chiral unitary symmetry class AIII. Such disorder produces no corrections to the conductivity to all orders and can be effectively gauged out at zero energy¹⁶. From the point of view of its transport properties, the system remains effectively clean and ballistic at all scales.

- (iii) If the only disorder is random mass (α_z), the Hamiltonian has a Bogolyubov – de Gennes symmetry $H = \sigma_1 H^T \sigma_1$ characteristic for the symmetry class D. Upon renormalization (43) the disorder coupling gets smaller and the system becomes effectively clean. This means the absence of the mean free path scale and hence of the diffusive transport regime.
- (iv) In the generic case, when more than one disorder type is present and all symmetries are broken, the symmetry class is unitary (A) and transport properties are the same as at the critical point of the quantum Hall transition.

We will concentrate on the first case (random potential) when the system eventually acquires a large parameter – dimensionless conductivity – and can be quantitatively described by the proper effective field theory – sigma model of the symplectic symmetry class. Our consideration in this part of the paper is closely related to that of Ref. 24.

Derivation of the sigma model with the source fields z from Eq. (6) is sketched in Appendix C. The symplectic sigma model operates with the matrix field Q of the size $4N \times 4N$, where N is the number of replicas. Apart from replica space, matrix Q has retarded-advanced (RA) and particle-hole (PH) structures. The former is similar to the matrix Green function while the latter is introduced in order to account for time-reversal symmetry of the problem. We will denote Pauli matrices in RA space by $\Lambda_{x,y,z}$. Two constraints are imposed on Q , namely, $Q^2 = 1$ and $Q = Q^T$. This yields the target space $Q \in O(4N)/O(2N) \times O(2N)$ characteristic for symplectic class systems. The sigma-model action is³⁹

$$S[Q] = \frac{\sigma}{16} \int d\mathbf{r} \text{Tr}(\nabla Q)^2. \quad (48)$$

Here σ is the dimensionless (in units e^2/h) conductivity of the two-dimensional disordered system. The source field is incorporated into boundary conditions,

$$Q|_{x=0} = \Lambda_z, \quad Q|_{x=L} = \Lambda_z \cos \phi + \Lambda_x \sin \phi. \quad (49)$$

The free energy of the system in the source field ϕ is expressed through the $N \rightarrow 0$ limit of the sigma-model partition function as

$$\Omega = \lim_{N \rightarrow 0} \frac{1}{N} \left(1 - \int DQ e^{-S[Q]} \right). \quad (50)$$

In a good metallic sample with $\sigma \gg 1$, the Q integral in Eq. (50) can be evaluated within the saddle point approximation. The action (48) is minimized by the following

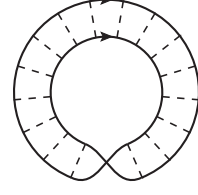


FIG. 5: Cooperon correction to the free energy in the diffusive limit.

configuration of the field Q :

$$Q_0 = U^{-1} \Lambda_z U, \quad U = \exp \left(i \Lambda_y \frac{\phi x}{2L} \right). \quad (51)$$

Replacing the integral in Eq. (50) with the value of the integrand at the saddle point, we obtain the semiclassical result for the full counting statistics,

$$\Omega_0 = \lim_{N \rightarrow 0} \frac{S[Q_0]}{N} = \frac{W \sigma \phi^2}{4L}. \quad (52)$$

This yields the Dorokhov distribution of transmission probabilities in diffusive two-dimensional system.⁴ In order to find corrections to this result, we take into account fluctuations of the field Q near its saddle-point value Q_0 . This is equivalent to the calculation of a Cooperon loop, Fig. 5, carried out in Ref. 24.

Small fluctuations of Q near the saddle point Q_0 are parametrized by the matrix B as (we write expressions involving B up to the second order)

$$Q = U^{-1} \Lambda_z \left(1 + B + \frac{B^2}{2} \right) U, \quad B = \begin{pmatrix} 0 & b \\ -b^T & 0 \end{pmatrix}. \quad (53)$$

This parametrization of Q automatically fulfils the conditions $Q^2 = 1$ and $Q = Q^T$. The sigma-model action expanded up to the second order in B takes the form

$$S[Q] = S[Q_0] - \frac{\sigma}{16} \int d\mathbf{r} \text{Tr} \left[(\nabla B)^2 - \frac{\phi^2}{4L^2} \{ \Lambda_x, B \}^2 \right]. \quad (54)$$

Curly braces denote anticommutator. Let us separate B into the parts commuting and anticommuting with Λ_x . These two parts do not couple to each other in the quadratic action (54) and only the former one couples to the source parameter ϕ . Thus we can constraint the matrix B by requiring its commutativity with Λ_x . In terms of b this yields $b = -b^T$ and the action becomes

$$S[Q] = S[Q_0] + \frac{\sigma}{8} \int d\mathbf{r} \text{Tr} \left[\nabla b \nabla b^T - \frac{\phi^2}{L^2} b b^T \right]. \quad (55)$$

This quadratic form is diagonalized in momentum representation. Component of momentum perpendicular to the leads takes quantized values $\pi n/L$ with positive integer n due to geometrical restrictions [boundary conditions (49) fix $b = 0$ at the interfaces with metallic leads].

Momentum parallel to the leads is continuous and unrestricted. For each value of the momentum there are $N(2N - 1)$ independent matrix elements in b . Calculating the Gaussian integral in Eq. (50) we obtain the free energy

$$\begin{aligned}\Omega &= \Omega_0 - \frac{W}{2} \sum_{n=1}^{\infty} \int \frac{dq_y}{2\pi} \ln(\pi^2 n^2 + q^2 L^2 - \phi^2) \\ &= \frac{W}{2L} \left[\frac{\sigma \phi^2}{2} - \sum_{n=1}^{\infty} \sqrt{\pi^2 n^2 - \phi^2} \right].\end{aligned}\quad (56)$$

In the result (56), the sum diverges at large n . The situation is similar to what we have encountered in the ballistic regime. Expanding the sum in powers of ϕ , we see that the most divergent term is ϕ -independent, while the next term multiplies ϕ^2 and diverges logarithmically. This is nothing but the weak antilocalization correction. It renormalizes the conductivity but does not deform the full counting statistics. Logarithmically divergent sum is cut at $n \sim L/l$ where l is the mean free path. At larger values of n the diffusive approximation (gradient expansion in the sigma model) breaks down. In terms of renormalized conductivity, the free energy reads

$$\Omega = \frac{W}{2L} \left[\frac{\tilde{\sigma} \phi^2}{2} - \sum_{n=1}^{\infty} \left(\sqrt{\pi^2 n^2 - \phi^2} - \pi n + \frac{\phi^2}{2\pi n} \right) \right],\quad (57)$$

$$\tilde{\sigma} = \sigma + \frac{1}{\pi} \ln \frac{L}{l} \approx \frac{1}{\pi} \ln \frac{L}{l}.\quad (58)$$

The bare value of conductivity, σ , is of order one and hence negligible in comparison with the large renormalizing logarithm. The sum over n in Eq. (57) is convergent and provides the deviation from semiclassical Dorokhov statistics of transmission probabilities.

In fact, a more rigorous procedure is to perform first a renormalization of the sigma model from the mean free path scale l to the scale $\sim L$. Then the free energy can be calculated perturbatively. It turns out, however, that this yields a result identical to the one obtained above within the perturbative analysis at the scale l . Indeed, the RG equation $d\sigma/d\ln L = 1/\pi$ will lead exactly to the renormalization of conductivity $\sigma \mapsto \tilde{\sigma}$, see Eq. (58). The consequent evaluation of the perturbative contribution to Ω yields Eq. (56) with σ replaced by $\tilde{\sigma}$ and the sum restricted to a finite (independent of L) number of terms. In other words, the renormalization shifts the logarithmic contribution to σ from the second to the first term in square brackets in Eq. (56).

Let us derive the distribution function $P(\lambda)$ from the free energy (57). Applying Eq. (12), we obtain the result in the form

$$P(\lambda) = \frac{W}{L} [\tilde{\sigma} + p(\lambda)],\quad (59)$$

$$p(\lambda) = \frac{1}{\pi} \sum_{n=1}^{\infty} \left[\operatorname{Re} \frac{\pi + 2i\lambda}{\sqrt{\pi^2 n^2 - (\pi + 2i\lambda)^2}} - \frac{1}{n} \right].\quad (60)$$

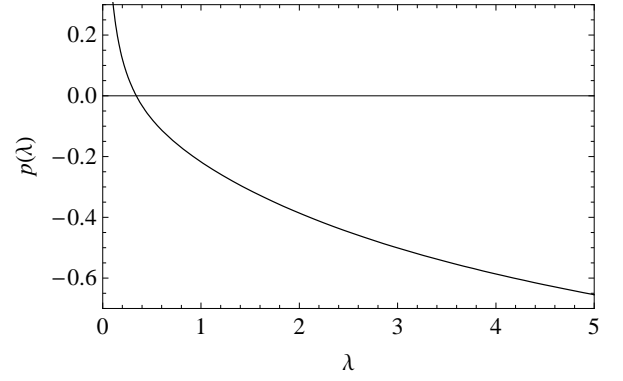


FIG. 6: Correction to the distribution of transmission eigenvalues in the diffusive limit.

At small values of λ , the sum in Eq. (60) is determined by the term with $n = 1$. In the opposite limit, the sum can be estimated by the corresponding integral with the help of Euler-Maclaurin formula. Thus we obtain the asymptotic expressions

$$p(\lambda) = \begin{cases} \sqrt{\frac{1}{8\pi\lambda}}, & \lambda \ll 1, \\ -\frac{1}{\pi} \ln \lambda, & \lambda \gg 1. \end{cases}\quad (61)$$

The function $p(\lambda)$ is shown in Fig. 6. It is qualitatively similar to the numerical result of Ref. 20.

Deviation from the semiclassical transport can be demonstrated by the correction to the Fano factor. With the help of Eq. (14), we obtain

$$F = \frac{1}{3} - \frac{2\zeta(3)}{\pi^3 \tilde{\sigma}} = \frac{1}{3} - \frac{0.244}{\ln(L/l)}.\quad (62)$$

A similar correction to the Fano factor was found numerically in Ref. 22. We compare the numerical results with Eq. (62) below.

In the case of weak scalar disorder (described by the coupling α_0), the system undergoes a continuous crossover from ballistic to diffusive transport regime as the size L grows. In both limiting cases, we encounter nearly Dorokhov distribution of transmission probabilities with small corrections, Eqs. (47) and (62), on both sides of the crossover. In the ballistic limit, we can formally introduce a dimensionless conductivity as $\sigma = (L/W)G/(e^2/h)$. Then the corrections to the Fano factor are expressed in terms of the conductivity

$$F = \frac{1}{3} - \begin{cases} \left(\frac{16\zeta(3)}{\pi^2} - \frac{8\pi^2}{45} \right) (\pi\sigma - 1)^2, & \pi\sigma - 1 \ll 1, \\ \frac{2\zeta(3)}{\pi^3 \sigma}, & \sigma \gg 1. \end{cases}\quad (63)$$

This Fano factor as a function of conductivity is shown in Fig. 7 together with numerical results from Ref. 22. In the numerical simulations, a single valley of graphene was

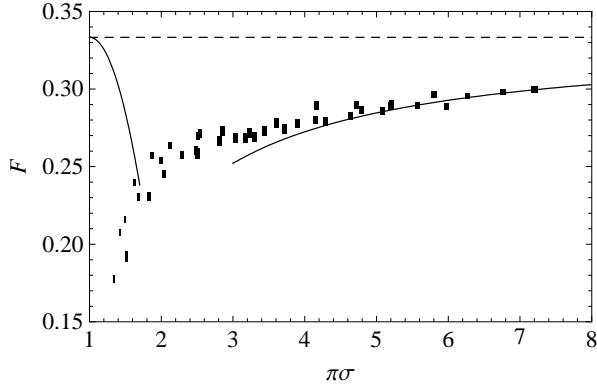


FIG. 7: Fano factor as a function of conductivity. Solid lines show ballistic and diffusive results (63). Dashed line corresponds to the asymptotic value $F = 1/3$. Solid symbols are numerical results from Ref. 22, the size of rectangles corresponds to the error estimate.

modeled using a finite-difference approach. By construction, disorder in Ref. 22 has the symmetry of scalar potential which does not mix the valleys. It is this symmetry (class AII) which is considered in the present section. Our results perfectly agree with the numerics in the diffusive limit (see Fig. 7) in the range $\pi\sigma \gtrsim 3$. On the ballistic side, the deviation is due to the non-universality of the ballistic transport. Specifically, the function $F(\sigma)$ depends crucially on the microscopic details of disorder. In the numerical analysis of Ref. 22, the model with strong scatterers was used, while in the present paper we adopt the model of weak Gaussian white-noise disorder. For theoretical predictions on electron transport in the presence of strong scatterers see Ref. 40.

An earlier numerical study of Ref. 20, based on the transfer-matrix description of the Dirac problem, reported the value of the Fano factor in the range $0.29 \div 0.30$ (for different samples) with the conductivity, $\pi\sigma$, of the largest systems varying from 6 to 10. This is consistent with our predictions for the diffusive transport regime

(see Fig. 7). The behavior of F in the ballistic regime is different due to the reasons described above (strong vs. weak disorder). A non-monotonous dependence $F(\sigma)$ at the Dirac point was also observed in Ref. 21.

The Fano factor is $1/3$ both in the clean and strongly disordered limits. In the crossover from ballistics to diffusion, the Fano factor strongly deviates from this universal value signifying the breakdown of the (pseudo-)diffusive description characterized by Dorokhov distribution of transmission probabilities.

VII. SUMMARY

We have studied the full counting statistics of the charge transport through an undoped graphene sheet in the presence of weak and smooth (not mixing valleys) disorder. We have identified deviations from the Dorokhov distribution of transmission probabilities both in ballistic [Eq. (45), (46)] and diffusive [Eqs. (59), (60)] regimes. In the former case, corrections are model-dependent while in the latter case only the symmetry of disorder matters. We have considered Gaussian white-noise disorder in the ballistic regime and potential disorder (symplectic symmetry class) in diffusive limit. Deviation from (pseudo-)diffusive transport always results in a negative correction to the Fano factor, $F < 1/3$. Our results are in good agreement with recent numerical simulations of electron transport in disordered graphene, see Fig. 7.

Acknowledgments

We are grateful to R. Danneau, P. San-Jose, and M. Titov for stimulating discussions and to C. Groth for providing us with the numerical data of Ref. 22. The work was supported by Rosnauka grant 02.740.11.5072 and by the EUROHORCS/ESF EURYI Award scheme (I.V.G.).

Appendix A: Matrix Green function

The full counting statistics of the electron transport is conveniently expressed in terms of the matrix Green function²⁵ in the external counting field $z = \sin^2(\phi/2)$, Eq. (6). For the clean graphene sample attached to perfect metallic leads, Fig. 1, this Green function satisfies the following equation:

$$\begin{pmatrix} \mu(x) - \sigma \mathbf{p} + i0 & -\sigma_x \sqrt{z} \delta(x) \\ -\sigma_x \sqrt{z} \delta(x-L) & \mu(x) - \sigma \mathbf{p} - i0 \end{pmatrix} \check{G}_0(\mathbf{r}, \mathbf{r}') = \delta(\mathbf{r} - \mathbf{r}'), \quad \mu(x) = \begin{cases} 0, & 0 < x < L, \\ +\infty, & x < 0 \text{ or } x > L. \end{cases} \quad (\text{A1})$$

Since the operator in the left-hand side of the above equation commutes with the y component of the momentum, we will first calculate the Green function in the mixed coordinate-momentum representation, $\check{G}_p(x, x')$. Inside the sample this function satisfies

$$\left[i\sigma_x \frac{\partial}{\partial x} - \sigma_y p \right] \check{G}_p(x, x') = \delta(x - x'). \quad (\text{A2})$$

We will look for a general solution of this equation in the form

$$\check{G}_p(x, x') = e^{\sigma_z p(x-L/2)} M e^{\sigma_z p(x'-L/2)}, \quad M = \begin{cases} M_<, & x < x', \\ M_>, & x > x'. \end{cases} \quad (\text{A3})$$

The chemical potential profile together with the infinitesimal terms $\pm i0$ in Eq. (A1) defines the boundary conditions for the Green function. The counting field z can also be incorporated into the boundary conditions. In terms of M_{\leq} we thus obtain

$$\begin{pmatrix} 1 & 1 & i\sqrt{z} & i\sqrt{z} \\ 0 & 0 & 1 & -1 \end{pmatrix} e^{-\sigma_z pL/2} M_< = 0, \quad \begin{pmatrix} 1 & -1 & 0 & 0 \\ -i\sqrt{z} & -i\sqrt{z} & 1 & 1 \end{pmatrix} e^{\sigma_z pL/2} M_> = 0. \quad (\text{A4})$$

Delta function in the right-hand side of Eq. (A2) yields a jump of the Green function at $x = x'$ which provides the relation

$$M_> - M_< = -i\sigma_x. \quad (\text{A5})$$

The matrices M_{\leq} , and hence the Green function, are completely determined by Eqs. (A4) and (A5),

$$M_{\leq} = \frac{-i}{2(\cosh^2 pL - z)} \begin{pmatrix} \cosh pL & z - \frac{\sinh 2pL}{2} & i\sqrt{z}e^{-pL} & i\sqrt{z} \\ z + \frac{\sinh 2pL}{2} & \cosh pL & i\sqrt{z} & i\sqrt{z}e^{pL} \\ i\sqrt{z}e^{pL} & i\sqrt{z} & -\cosh pL & -z - \frac{\sinh 2pL}{2} \\ i\sqrt{z} & i\sqrt{z}e^{-pL} & -z + \frac{\sinh 2pL}{2} & -\cosh pL \end{pmatrix} \pm \frac{i\sigma_x}{2}. \quad (\text{A6})$$

Fourier transform in p yields the Green function in the full coordinate representation. To facilitate further calculations, we decompose this Green function into the following product of matrices:

$$\check{G}_0(x, x'; y) = \frac{1}{4L} \check{U}(x) \check{\Lambda} \begin{pmatrix} i \cosh \frac{\phi y}{2L} & \sinh \frac{\phi y}{2L} \\ \sinh \frac{\phi y}{2L} & -i \cosh \frac{\phi y}{2L} \end{pmatrix}_{RA} \begin{pmatrix} \frac{1}{\sin \frac{\pi}{2L}(x+x'+iy)} & \frac{1}{\sin \frac{\pi}{2L}(x-x'+iy)} \\ \frac{1}{\sin \frac{\pi}{2L}(x-x'-iy)} & \frac{1}{\sin \frac{\pi}{2L}(x+x'-iy)} \end{pmatrix}_{\sigma} \check{\Lambda} \check{U}^{-1}(x'), \quad (\text{A7})$$

$$\check{\Lambda} = \begin{pmatrix} \sigma_z & 0 \\ 0 & 1 \end{pmatrix}_{RA}, \quad \check{U}(x) = \begin{pmatrix} \sin \frac{\phi(L-x)}{2L} & \cos \frac{\phi(L-x)}{2L} \\ i \cos \frac{\phi x}{2L} & i \sin \frac{\phi x}{2L} \end{pmatrix}_{RA}. \quad (\text{A8})$$

Here we have used the source angle ϕ defined by $z = \sin^2(\phi/2)$. The matrices $\check{U}(x)$ and $\check{U}^{-1}(x')$ operate in the retarded-advanced space only and hence commute with any disorder operators placed between the Green functions. As a result, factors \check{U} and \check{U}^{-1} drop from expressions for any closed diagrams. The matrices $\check{\Lambda}$ in the above equation allow us to decompose the Green function into a direct product of the two operators acting in the RA space and in the sublattice space.

Appendix B: Energy correction to the full counting statistics

In this appendix we evaluate the diagram Fig. 2 for the lowest energy correction to $\Omega(\phi)$. Substituting Green function (A7) into Eq. (19) and performing rescaling of integration variables we obtain

$$\Omega_{\epsilon} = \frac{WL\epsilon^2}{4} \int_0^1 dx \, dx' \int_{-\infty}^{\infty} dy \cosh(\phi y) \left[\frac{1}{\cosh(\pi y) - \cos \pi(x+x')} - \frac{1}{\cosh(\pi y) - \cos \pi(x-x')} \right]. \quad (\text{B1})$$

The first (second) term in square brackets depends only on sum (difference) of x and x' . This allows us to integrate over the difference (sum) of these variables. After some shifts of variables the remaining integral takes the form

$$\Omega_{\epsilon} = -\frac{WL\epsilon^2}{2} \int_0^1 du \, u \sin \frac{\pi u}{2} \int_{-\infty}^{\infty} \frac{dy \cosh(\phi y)}{\cosh^2(\pi y) - \sin^2(\pi u/2)} = -\frac{WL\epsilon^2}{2 \sin(\phi/2)} \int_0^1 du \, u \frac{\sin(\phi u/2)}{\cos(\pi u/2)}. \quad (\text{B2})$$

The last expression is the result of y integration. It can be performed, e.g., by closing the integration contour and summing up residues in the upper half-plane of imaginary y . In order to make this sum convergent, one has to add a weak damping factor by an infinitesimal imaginary shift of ϕ .

We proceed with the last integral in Eq. (B2) by representing $1/\cos(\pi u/2)$ as a Fourier series

$$\Omega_\epsilon = \frac{2WL\epsilon^2}{\sin(\phi/2)} \frac{\partial}{\partial\phi} \int_0^1 du \cos \frac{\phi u}{2} \sum_{n=0}^{\infty} (-1)^n \cos[\pi u(n+1/2)]. \quad (\text{B3})$$

Convergence of this Fourier series should also be justified by a proper damping factor. This does not change the final result of the calculation hence we omit such extra factors for simplicity. Performing the integration over u we obtain

$$\Omega_\epsilon = \frac{2WL\epsilon^2}{\sin(\phi/2)} \frac{\partial}{\partial\phi} \cos \frac{\phi}{2} \sum_{n=0}^{\infty} \left[\frac{1}{\pi(2n+1)+\phi} + \frac{1}{\pi(2n+1)-\phi} \right]. \quad (\text{B4})$$

The sum over n diverges logarithmically. However, this divergence is independent of ϕ and hence does not influence any observable quantities, which are expressed as derivatives of the free energy. We can easily get rid of the divergent part by subtracting a similar sum over n with $\phi = 0$. This yields the final result

$$\begin{aligned} \Omega_\epsilon &= \frac{2WL\epsilon^2}{\sin(\phi/2)} \frac{\partial}{\partial\phi} \cos \frac{\phi}{2} \sum_{n=0}^{\infty} \left[\frac{1}{\pi(2n+1)+\phi} + \frac{1}{\pi(2n+1)-\phi} - \frac{2}{\pi(2n+1)} \right] \\ &= -\frac{W}{\pi L} \frac{(\epsilon L)^2}{\sin \frac{\phi}{2}} \frac{\partial}{\partial\phi} \left\{ \cos \frac{\phi}{2} \left[\psi \left(\frac{\pi+\phi}{2\pi} \right) + \psi \left(\frac{\pi-\phi}{2\pi} \right) + 4\ln 2 + 2\gamma \right] \right\}. \end{aligned} \quad (\text{B5})$$

Here ψ is the digamma function and γ is the Euler-Mascheroni constant. The last expression yields Eq. (20) of the main text (where we drop the unobservable constant).

Appendix C: Derivation of the sigma model

In order to carry out a parametrically controlled derivation of the sigma model, it is convenient to consider a modified problem with $n \gg 1$ flavours of Dirac fermions. To perform the disorder average of the free energy, we also introduce N replicas. (Alternatively, one can use supersymmetry. As we will treat the sigma model perturbatively, the two approaches are fully equivalent.)

The derivation of the sigma model starts with the fermionic action generating the matrix Green function (6).

$$S[\phi, \phi^*] = \int d\mathbf{r} \sum_{a,b,\alpha} \phi_a^{\alpha\dagger} \left(\left\{ i0\Lambda_z - \boldsymbol{\sigma}\mathbf{p} - \sqrt{z}\sigma_x [\Lambda_+\delta(x) + \Lambda_-\delta(x-L)] \right\} \delta_{ab} - V_{ab}(\mathbf{r}) \right) \phi_b^\alpha. \quad (\text{C1})$$

Here $\Lambda_\pm = (\Lambda_x \pm i\Lambda_y)/2$ are matrices operating in RA space. This action is the functional of two independent Grassmann two-component (in σ space) vector fields ϕ and ϕ^* . Lower indices, a and b , refer to flavours while the upper index α enumerates replicas. Overall, there are $4nN$ independent Grassmann variables in the Lagrangian. The random matrix V_{ab} is symmetric, that insures the time-reversal symmetry of the model. We assume Gaussian white-noise statistics for the matrix V defined by the correlator

$$\langle V_{ab}(\mathbf{r}) V_{cd}(\mathbf{r}') \rangle = \frac{2\pi\alpha_0}{n} [\delta_{ac}\delta_{bd} + \delta_{ad}\delta_{bc}] \delta(\mathbf{r} - \mathbf{r}'). \quad (\text{C2})$$

Using the time-reversal symmetry, we rewrite the action in terms of the single four-component field ψ (and its charge-conjugate version $\bar{\psi}$, that is linearly related to ψ):

$$\psi = \frac{1}{\sqrt{2}} \begin{pmatrix} \phi \\ i\sigma_y \phi^* \end{pmatrix}, \quad \bar{\psi} = i\psi^T \sigma_y \tau_x = \frac{1}{\sqrt{2}} (\phi^\dagger, i\phi^T \sigma_y). \quad (\text{C3})$$

This introduces an additional particle-hole (PH) structure of the fields. Pauli matrices operating in PH space are denoted by $\tau_{x,y,z}$. Bar denotes the charge conjugation operation which has two important properties: $\bar{\psi}_1 \psi_2 = \bar{\psi}_2 \psi_1$ and $(\psi_1 \bar{\psi}_2)^T = \tau_x \sigma_y \psi_2 \bar{\psi}_1 \sigma_y \tau_x$. The action takes the following form in terms of ψ :

$$S[\psi] = \int d\mathbf{r} \sum_{a,b,\alpha} \bar{\psi}_a^\alpha \left(\left\{ i0\Lambda_z - \boldsymbol{\sigma}\mathbf{p} - \sqrt{z}\sigma_x [\rho_+\delta(x) + \rho_-\delta(x-L)] \right\} \delta_{ab} - V_{ab}(\mathbf{r}) \right) \psi_b^\alpha. \quad (\text{C4})$$

In this expression we have introduced the notation $\rho_{\pm} = (\Lambda_x \tau_z \pm i \Lambda_y)/2$.

Now we are ready to average e^{-S} over the Gaussian disorder distribution with the correlator (C2). This yields an effective action with the quartic term. Using the above-mentioned properties of charge conjugation, we recast the action in the form

$$S[\psi] = \int d\mathbf{r} \left[\sum_{a,\alpha} \bar{\psi}_a^\alpha \left\{ i0\Lambda_z - \boldsymbol{\sigma}\mathbf{p} - \sqrt{z}\sigma_x [\rho_+\delta(x) + \rho_-\delta(x-L)] \right\} \psi_a^\alpha + \frac{2\pi\alpha_0}{n} \sum_{a,b,\alpha,\beta} \text{Tr} \psi_a^\alpha \bar{\psi}_a^\beta \psi_b^\beta \bar{\psi}_b^\alpha \right]. \quad (\text{C5})$$

Next, we decouple the quartic term introducing an auxiliary $8N \times 8N$ matrix R by the Hubbard-Stratonovich transformation. This yields the action

$$S[R, \psi] = \int d\mathbf{r} \left[\frac{n\gamma^2}{8\pi\alpha_0} \text{Tr} R^2 + \sum_{a,\alpha,\beta} \bar{\psi}_a^\alpha \left(i\gamma R_{\alpha\beta} - \left\{ \boldsymbol{\sigma}\mathbf{p} + \sqrt{z}\sigma_x [\rho_+\delta(x) + \rho_-\delta(x-L)] \right\} \delta_{\alpha\beta} \right) \psi_a^\beta \right]. \quad (\text{C6})$$

Parameter γ is an arbitrary number at this stage, its value will be fixed later. Matrix $R_{\alpha\beta}$ couples to the product $\sum_a \psi_a^\alpha \bar{\psi}_a^\beta$. This allows us to impose the corresponding symmetry constraint on the matrix R : $R = \sigma_y \tau_x R^T \sigma_y \tau_x$. Finally, we integrate out the fermionic fields and obtain the action operating with the matrix R only,

$$S[R] = \frac{n}{2} \mathbf{Tr} \left(\frac{\gamma^2 R^2}{4\pi\alpha_0} - \ln \left\{ i\gamma R - \boldsymbol{\sigma}\mathbf{p} - \sqrt{z}\sigma_x [\rho_+\delta(x) + \rho_-\delta(x-L)] \right\} \right). \quad (\text{C7})$$

The bold ‘ \mathbf{Tr} ’ symbol implies the full operator trace including integration over space coordinates.

Derivation of the sigma model proceeds with the saddle-point analysis of the action (C7) in the absence of the source field z . We first look for a diagonal and spatially constant matrix R minimizing the action. The saddle-point equation is identical to the self-consistent Born approximation (SCBA) equation for the self energy $-i\gamma R$,

$$-i\gamma R = 2\pi\alpha_0 \int \frac{d\mathbf{p}}{(2\pi)^2} (i\gamma R - \boldsymbol{\sigma}\mathbf{p})^{-1}. \quad (\text{C8})$$

We fix γ to be the imaginary part of the SCBA self energy, $\gamma = \Delta e^{-1/\alpha_0}$ with Δ being ultraviolet energy cut-off (band width). Then the saddle-point configuration for the matrix R is simply $R = \Lambda_z$. This fixes the boundary conditions for the matrix R at the contacts. Since the leads are very good metals and fluctuations of R are strongly suppressed there, $R = \Lambda_z$ for $x < 0$ and $x > L$.

The matrix $R = \Lambda_z$ is not the only saddle point of the action (C7). Other configurations minimizing the action can be obtained by rotations $R = T^{-1} \Lambda_z T$ with any matrix T which commutes with $\boldsymbol{\sigma}\mathbf{p}$ and preserves the constraint $R = \sigma_y \tau_x R^T \sigma_y \tau_x$. Matrix T , and hence R , is trivial in σ space. This allows us to reduce the dimension of R to $4N \times 4N$ operating in Λ , τ , and replicas only. The saddle manifold generated by matrices T is $O(4N)/O(2N) \times O(2N)$.

Let us now restore the source term in the action and establish boundary conditions for R . The matrix R has a jump at the interfaces with the leads due to the delta functions in the action (C7). However, we can eliminate these jumps by a proper gauge transformation. Let us perform a rotation $R = A \tilde{R} A^{-1}$ with an x -dependent matrix A . The action acquires the following form in terms of \tilde{R} :

$$S[\tilde{R}] = \frac{n}{2} \mathbf{Tr} \left[\frac{\gamma^2 \tilde{R}^2}{2\pi\alpha_0} - \ln \left(i\gamma \tilde{R} - \boldsymbol{\sigma}\mathbf{p} + i\sigma_x A^{-1} \left\{ \frac{\partial A}{\partial x} + i\sqrt{z} [\rho_+\delta(x) + \rho_-\delta(x-L)] A \right\} \right) \right]. \quad (\text{C9})$$

The source field drops from this action if we choose A such that the expression in curly braces vanishes. This yields

$$A = \begin{cases} 1, & x < 0, \\ 1 - i\sqrt{z}\rho_+, & 0 < x < L, \\ (1 - i\sqrt{z}\rho_-)(1 - i\sqrt{z}\rho_+), & x > L. \end{cases} \quad (\text{C10})$$

Note that the matrix \tilde{R} , defined with the help of the above matrix A , fulfils the condition $\tilde{R} = \tau_x \tilde{R}^T \tau_x$. Since delta functions disappear from the action, we can infer that \tilde{R} is continuous at the interfaces with the leads. In the left lead we have $R = \tilde{R} = \Lambda_z$. This is the left boundary condition for the matrix \tilde{R} . The right boundary condition is fixed by the identities $\tilde{R} = A^{-1} R A$ and $R = \Lambda_z$ for $x > L$. This yields

$$\tilde{R}(L) = (1 - 2z)\Lambda_z + iz^{3/2}\Lambda_x + \sqrt{z}(2 - z)\Lambda_y \tau_z. \quad (\text{C11})$$

We can further simplify this bulky expression by performing a constant rotation $\tilde{R} = B^{-1}QB$ with the matrix

$$B = \frac{\tau_z - \tau_y}{2\sqrt{2}} \left[(1-z)^{-1/4}(1 + \Lambda_z \tau_z) - i(1-z)^{1/4}(1 - \Lambda_z \tau_z) \right]. \quad (\text{C12})$$

After such a rotation the action and boundary conditions become

$$S[Q] = \frac{n}{2} \text{Tr} \left[\frac{\gamma^2 Q^2}{2\pi\alpha_0} - \ln(i\gamma Q - \sigma \mathbf{p}) \right], \quad (\text{C13})$$

$$Q(0) = \Lambda_z, \quad Q(L) = \Lambda_z \cos \phi + \Lambda_x \sin \phi. \quad (\text{C14})$$

Thus we have reduced the boundary conditions to the form (49). The matrix B is chosen such that $B^T B = \tau_x$. Hence the matrix Q obeys the symmetry constraint $Q = Q^T$.

The last step of the sigma-model derivation is the gradient expansion in Eq. (C13). This expansion is straightforward for the real part of the action³⁹

$$\text{Re } S[Q] = -\frac{n}{4} \text{Tr} \ln(i\gamma Q - \sigma \mathbf{p})(-i\gamma Q - \sigma \mathbf{p}) = -\frac{n}{4} \text{Tr} \ln(p^2 + \gamma^2 + \gamma \sigma \nabla Q) \simeq \frac{n}{16\pi} \text{Tr}(\nabla Q)^2. \quad (\text{C15})$$

The Drude conductivity of the two-dimensional sample with n flavours of massless Dirac fermions at the Dirac point is $(n/\pi)(e^2/h)$. With the dimensionless conductivity $\sigma = n/\pi$, we finally obtain Eq. (48) supplemented by the boundary conditions (49).

-
- ¹ A. K. Geim and K. S. Novoselov, *Nature Materials* **6**, 183 (2007).
² A. H. Castro Neto, F. Guinea, N. M. R. Peres, K. S. Novoselov, and A. K. Geim, *Rev. Mod. Phys.* **81**, 109 (2009).
³ M. I. Katsnelson, *Eur. Phys. J. B* **51**, 157 (2006).
⁴ O. N. Dorokhov, *Zh. Eksp. Teor. Fiz.* **85**, 1040 (1983) [*Sov. Phys. JETP* **58**, 606 (1983)].
⁵ J. Tworzydło, B. Trauzettel, M. Titov, A. Rycerz, and C. W. J. Beenakker, *Phys. Rev. Lett.* **96**, 246802 (2006).
⁶ S. Ryu, C. Mudry, A. Furusaki, and A. W. W. Ludwig, *Phys. Rev. B* **75**, 205344 (2007).
⁷ C. W. J. Beenakker, *Rev. Mod. Phys.* **80**, 1337 (2008).
⁸ C. W. J. Beenakker, *Rev. Mod. Phys.* **69**, 731 (1997).
⁹ H. B. Heersche P. Jarillo-Herrero, J. B. Oostinga, L. M. K. Vandersypen, A. F. Morpurgo, *Nature* **446**, 56 (2007).
¹⁰ R. Danneau, F. Wu, M.F. Craciun, S. Russo, M. Y. Tomi, J. Salmilehto, A. F. Morpurgo, and P. J. Hakonen, *Phys. Rev. Lett.* **100**, 196802 (2008); *J. Low Temp. Phys.* **153**, 374 (2008); *Solid State Comm.* **149**, 1050 (2009).
¹¹ F. Miao, S. Wijeratne, Y. Zhang, U. C. Coskun, W. Bao, and C. N. Lau, *Science* **317**, 1530 (2007).
¹² Xu Du, I. Skachko, A. Barker, E. Y. Andrei, *Nature Nanotech.* **3**, 491 (2008).
¹³ K. I. Bolotin, F. Ghahari, M. D. Shulman, H. L. Stormer, P. Kim, *Nature (London)* **462**, 196 (2009).
¹⁴ J. H. Bardarson, J. Tworzydło, P. W. Brouwer, and C. W. J. Beenakker, *Phys. Rev. Lett.* **99**, 106801 (2007).
¹⁵ M. Titov, *Europhys. Lett.* **79**, 17004 (2007).
¹⁶ A. Schuessler, P. M. Ostrovsky, I. V. Gornyi, and A. D. Mirlin, *Phys. Rev. B* **79**, 075405 (2009).
¹⁷ K. S. Novoselov, A. K. Geim, S. V. Morozov, D. Jiang, M. I. Katsnelson, I. V. Grigorieva, S. V. Dubonos, and A. A. Firsov, *Nature (London)* **438**, 197 (2005).
¹⁸ P. M. Ostrovsky, I. V. Gornyi, and A. D. Mirlin, *Phys. Rev. Lett.* **98**, 256801 (2007); *Eur. Phys. J. Spec. Top.* **148**, 63 (2007).
¹⁹ K. Nomura, M. Koshino, and S. Ryu, *Phys. Rev. Lett.* **99**, 146806 (2007).
²⁰ P. San-Jose, E. Prada, and D. S. Golubev, *Phys. Rev. B* **76**, 195445 (2007).
²¹ C. H. Lewenkopf, E. R. Mucciolo, and A. H. Castro Neto, *Phys. Rev. Lett.* **77**, 081410R (2008).
²² J. Tworzydło, C. W. Groth, and C. W. J. Beenakker, *Phys. Rev. B* **78**, 235438 (2008).
²³ L. DiCarlo, J. R. Williams, Yiming Zhang, D. T. McClure, C. M. Marcus, *Phys. Rev. Lett.* **100**, 156801 (2008).
²⁴ Yu. V. Nazarov, *Phys. Rev. B* **52**, 4720 (1995).
²⁵ Yu. V. Nazarov, *Phys. Rev. Lett.* **73**, 134 (1994).
²⁶ Y. Zhang, Y.-W. Tan, H. L. Stormer, and P. Kim, *Nature (London)* **438**, 201 (2005).
²⁷ P. M. Ostrovsky, I. V. Gornyi, and A. D. Mirlin, *Phys. Rev. B* **77**, 195430 (2008).
²⁸ F. V. Tikhonenko, D. W. Horsell, R. V. Gorbachev, and A. K. Savchenko, *Phys. Rev. Lett.* **100**, 056802 (2008); D. W. Horsell, A. K. Savchenko, F. V. Tikhonenko, K. Kechedzhi, I. V. Lerner, V. I. Fal'ko, *Solid State Comm.* **149**, 1041 (2009); F. V. Tikhonenko, A. A. Kozikov, A. K. Savchenko, R. V. Gorbachev, *Phys. Rev. Lett.* **103**, 226801 (2009).
²⁹ T. Ando, *J. Phys. Soc. Jpn* **75**, 074716 (2006).
³⁰ K. Nomura and A. H. MacDonald, *Phys. Rev. Lett.* **96**, 256602 (2006).
³¹ D. V. Khveshchenko, *Phys. Rev. B* **75**, 241406(R) (2007).
³² P. M. Ostrovsky, I. V. Gornyi, and A. D. Mirlin, *Phys. Rev. B* **74**, 235443 (2006).
³³ Y.-W. Tan, Y. Zhang, H. L. Stormer, and P. Kim, *Eur. Phys. J. Special Topics*, **148**, 15 (2007).
³⁴ An alternative possibility is that the dominant disorder is formed by resonant scatterers preserving the chiral symmetry^{32,40}. A detailed analysis of the evolution from ballistics to diffusion in this model will be published else-

where.

- ³⁵ The result (30) is twice smaller than the correction obtained in Ref. 16 within the transfer-matrix approach. The reason for this discrepancy is that in the latter case ultraviolet divergency was regulated by introducing a finite correlation length in the y direction only. This resulted in the angle average $\langle \delta_y^2 / \delta^2 \rangle = 1$ being twice larger than for the isotropic model adopted in the current paper, $\langle \delta_y^2 / \delta^2 \rangle = 1/2$.
- ³⁶ I. L. Aleiner and K. B. Efetov, Phys. Rev. Lett. **97**, 236801 (2006).
- ³⁷ M. R. Zirnbauer, J. Math. Phys. **37**, 4986 (1996); A. Altland and M. R. Zirnbauer, Phys. Rev. B **55**, 1142 (1997).
- ³⁸ F. Evers and A. D. Mirlin, Rev. Mod. Phys. **80**, 1355 (2008).
- ³⁹ The sigma-model action contains also an imaginary Z_2 topological term¹⁸ omitted in Eq. (48). This term is crucial for ensuring topological protection from Anderson localization at small σ . Here we are focusing, however, on the range of large σ , where the effect of topological term is exponentially small and can be discarded.
- ⁴⁰ M. Titov, P. M. Ostrovsky, I. V. Gornyi, A. Schuessler, and A. D. Mirlin, Phys. Rev. Lett. **104**, 076802 (2010).